Experimental and Numerical Investigation of Flow and Combustion in a Single Element Rocket Combustor using GH2/GOX and GCH4/GOX as Propellants

By CHRISTOF ROTH,[1] SIMONA SILVESTRI,[1] NIKOLAOS PERAKIS[1] and OSKAR HAIDN[1]

[1] *Technical University of Munich, Institute for Turbomachinery and Flight Propulsion, Germany*

Wall pressure and wall temperature measurements in a lab-scale rocket combustor are presented. The combustor has a circular cross-section with an inner diameter of 12 mm and a total length of 305 mm and features a single shear coaxial injector element. It is operated using gaseous oxygen as oxidizer and either gaseous hydrogen or gaseous methane as fuel. The experiments were conducted at a pressure of 20 bars. Four operating points distinguished by the oxidizer to fuel ratio (O/F) were tested for methane, O/F = 2.2, 2.6, 3.0 and 3.4, and three for hydrogen, O/F = 4.4, 5.2 and 5.9. The wall heat flux was reconstructed from the temperature measurements as an indication of the heat leaving the combustor. Two different combustion efficiencies were calculated and their results discussed. One is an overall efficiency for the thrust chamber, the other one an injector related energy release efficiency. In addition to the experiments for the methane O/F = 2.6 and the hydrogen O/F = 5.9 case numerical simulations using a CFD RANS model were conducted. The results are discussed and compared to the experimental data.

Key Words: rocket engines, experimental, numerical

Nomenclature

A	:	area
CEA	:	Chemical Equilibrium with Applications
CFD	:	computational fluid dynamics
GFU	:	gaseous fuel
GCH4	:	gaseous methane
GH2	:	gaseous hydrogen
GOX	:	gaseous oxygen
JANNAF	:	Joint Army Navy NASA Air Force
JAXA	:	Japan Aerospace Exploration Agency
LOX	:	liquid oxygen
$\dot{m}$	:	.. mass flow rate
PDF	:	Probability Density Function
RANS	:	Reynolds-averaged Navier-Stokes
TCI	:	turbulence-chemistry interaction

Subscripts

c	:	combustion
fu	:	fuel
id	:	ideal
ox	:	oxidizer
th	:	throat
w	:	wall

1. Introduction

Experiments conducted to investigate the performance and the wall heat flux of a gas/gas single element rocket combustor are presented and discussed. The experiments were conducted as part of the national research program SFB/TRR-40 on the "Technological Foundations for the Design of Thermally and Mechanically Highly Loaded Components of Future Space Transportation Systems".

In the presented study two different propellant combinations GH2/GOX and GCH4/GOX were tested. Hydrogen has been used traditionally in liquid rocket engines for launcher applications mainly due to its high specific impulse. In recent years methane has been investigated as a viable alternative having the highest specific impulse among hydrocarbon fuels and displaying other desirable characteristics from a system point of view,[1] e.g. space storability or low toxicity. European and Russian industries[2] cooperate to conceive a LOX/GCH4 engine for booster applications. Jaxa[3] conducts hot-firing tests on a LOX/GCH4 rocket engine for an upper stage system. Purdue University[4] focuses the attention on LOX/CH4 expander cycle engines. However, experience with methane combustion under rocket combustor conditions as well as experience with gas/gas injectors is still limited. Here the goal was to characterize the wall pressure and heat flux distribution for methane as well as hydrogen using the same hardware configuration and injector setup. This is done for multiple different operating points as far as oxygen to fuel ratio is concerned and serves as basis for an ongoing CFD model validation.

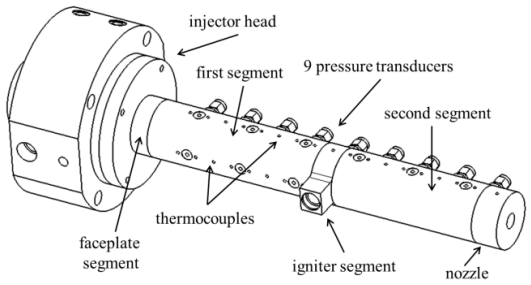

Fig. 1 Combustor schematic.

In addition, preliminary results from a CFD model for one operating point of each propellant combination are presented. In this case the CFD was done in order to help improve the understanding of the physical and chemical processes inside the combustor and support with the interpretation of the experimental data. The numerical calculations are viewed as support to the experiments.

2. Experimental Setup

In this section the experimental setup, i.e. the hardware configuration and the operating conditions are described. In total, results for seven load points are presented, four are methane combustion cases and three are hydrogen. All load points were investigated experimentally.

2.1. Hardware Configuration

The combustion chamber is a modular heat sink hardware made of oxygen-free high conductivity copper. Due to the modular design the chamber length and configuration can be varied by inserting or removing different chamber segments. The configuration used for the presented results is depicted in Fig. 1.

The total chamber length is 305 mm and the inner diameter is 12 mm. The nozzle has a conical shape with a throat diameter of 7.6 mm. Therefore the contraction ratio of the configuration is 2.5, which is close to actual flight hardware (Vulcain: 2.5, Aestus: 2.38).[5] This ensures a similar Mach number in the combustor compared to that of the actual flight engines.

The hardware is equipped with several thermocouples along the chamber wall in axial direction. These are placed in short distance (1-3 mm) from the hot gas wall side and give an indication of the material heat up during the hot firing tests. The measurements are also used to reconstruct the experimental wall heat flux according to the inverse heat transfer method described in Celano et al.[6]

The wall pressure distribution is measured by nine pressure transducers mounted along the chamber wall. From their readings the axial evolution of the chamber pressure, which is related to the heat release, is obtained. The nominal chamber pressure, defined as the total chamber pressure at the throat, is calculated from the last pressure measurement in the combustor using the simplified JANNAF procedure.[7]

The injector used in the investigated configuration is a coaxial shear type injector. A schematic is shown in Fig. 2. The oxidizer post tip is flush mounted with the faceplate, i.e. no recess is configured. The post tip is not tapered. The characteristic dimensions for the injector are given in Table 1. The element wall distance is equal to the outer radius of the hydrogen annulus, i.e. 3 mm.

Table 1 Injector dimensions.

GOX diameter	d_i	=	4 mm
GFU outer diameter	d_o	=	6 mm
GOX post thickness	t	=	0.5 mm
Recess length	R	=	0 mm

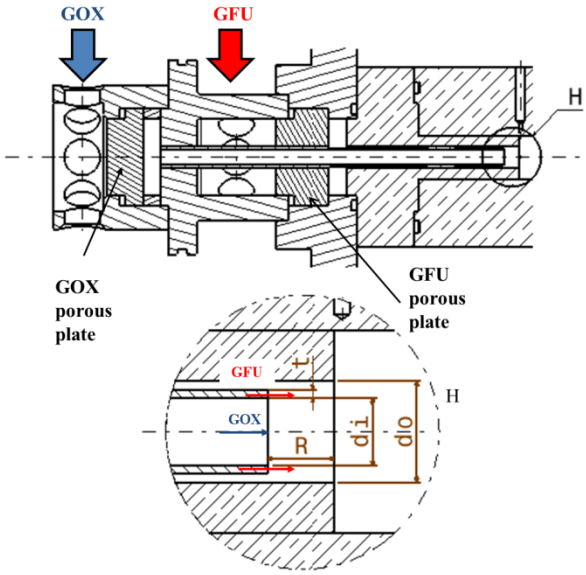

Fig. 2 Schematic of the injector.

2.2. Operating Conditions

The operating points are defined by the nominal combustion pressure and the oxidizer to fuel ratio of the propellants. These values are linked to the propellant mass flow rates by the equations:

$$\dot{m} = \frac{p_c A_{th}}{c^*} \tag{1}$$

and

$$O/F = \frac{\dot{m}_{ox}}{\dot{m}_{fu}} \tag{2}$$

In the experiments the mass flow rates are set by sonic orifices in the feed lines and the upstream pressure. The orifices in the feed lines to the main injector have been manufactured with appropriate diameters and calibrated with nitrogen using a Coriolis flow meter prior to the test campaign. The actual mass flows are calculated from the recorded pressure, temperature signals and the orifice calibration data after the test, assuming sonic flow condition in the orifices. The mass flow rates for the presented load points are shown in Fig. 3.

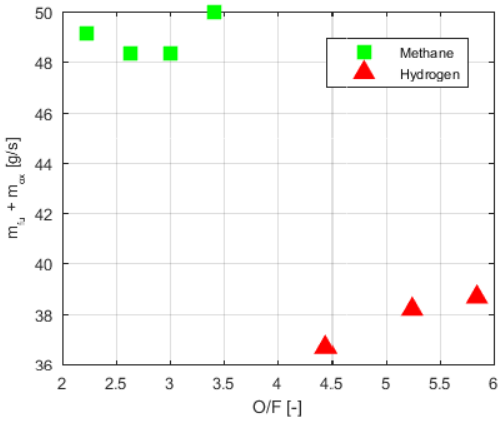

Fig. 3 Mass flow rates for all load points.

With the mass flow rates from the experiments, the expected theoretical combustion pressure at 100 % combustion efficiency can be determined using Equation (1). The value of the characteristic velocity c^* is determined using NASA's Chemical Equilibrium with Applications (CEA) code[7].

The actual measured combustion pressure is calculated from the last pressure measurement in the combustor using the simplified JANNAF procedur.[8]
Both values are shown in Fig. 4.

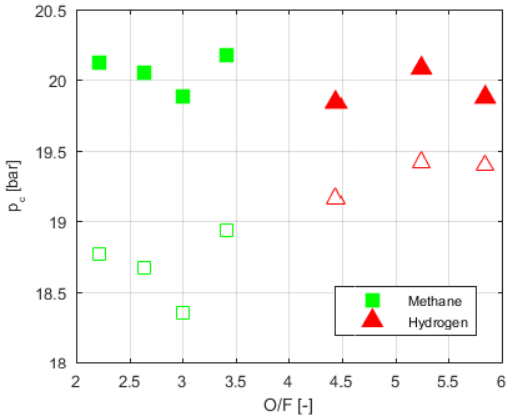

Fig. 4 Theoretical (filled markers) and measured (non-filled markers) nominal combustion pressure.

The measured injection temperatures of the propellants are summarized in Table 2. The measurement location is in the reservoir downstream of the porous plate for the oxidizer as well as the fuel.

Table 2 Injection temperatures.

Load Point	T_{fu} [K]	T_{ox} [K]
CH4: 2.2	268	276
CH4: 2.6	269	275
CH4: 3.0	270	274
CH4: 3.4	271	273
H2: 4.4	286	284
H2: 5.2	285	281
H2: 5.9	285	280

3. Experimental results

In this section the experimental results are presented and discussed. The data presented is focused on measured and from measurements derived quantities that are commonly used for the validation of CFD tools for the prediction of wall heat loads and performance characteristics of rocket combustors. Two different combustion efficiencies were calculated and their results discussed. One is an overall efficiency for the thrust chamber, the other one an injector related energy release efficiency.

3.1. Wall pressure distribution

The pressure along the combustor wall was measured using a series of equally spaced pressure transducers. The wall pressure measurements for the presented load points are given in Fig. 5.

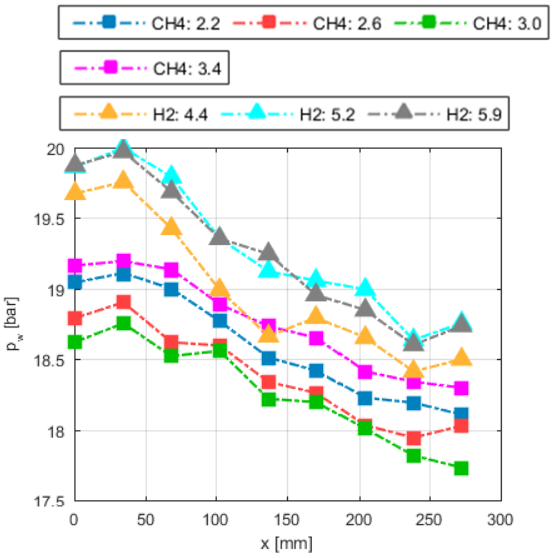

Fig. 5 Wall pressure distribution.

The general shape of the pressure distribution is similar for all tests. After a short rise of the wall pressure from the first to the second pressure sensor, which is caused by recirculating hot gas near the faceplate, the pressure drops throughout the chamber, which causes the acceleration of the hot gas flow. The pressure level for the hydrogen cases is higher than for the methane cases. Since the expected theoretical pressures are close to the methane ones this gives a first indication of increased combustion efficiency although in theory a higher integrated heat loss in the methane case could also explain this behavior.

3.2. Wall heat flux

The correct prediction of the heat loss in a rocket combustor is a major task in the design stage, as it is fundamental for the layout of the cooling system. To predict different design configurations using CFD models these should be validated using test data. The wall heat flux for all tests presented here was calculated from the thermocouple readings using an inverse heat transfer method. Only the thermocouples inside the cylindrical part of the combustor were used in this method and only the results for this part are presented here. The results are shown in Fig. 6.

The heat flux distribution for the two different propellant combinations shows significant differences. In the case of methane the heat flux rises gradually and seems to reach a plateau at around 200 mm from the faceplate and is slightly dropping afterwards, indicating the end of the combustion process. Hydrogen in contrast shows a steep jump at 70 mm followed by a plateau. The plateau value for hydrogen is around 9 MW/m², while the value for methane is around 7 MW/m².

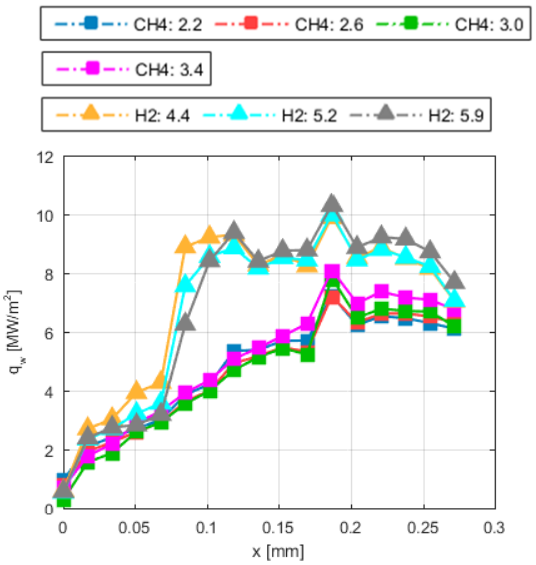

Fig. 6 Wall heat flux distribution.

To quantify the total heat loss through the chamber wall the integrated heat flux can be determined. The values of the integrated heat flux are summarized in Table 3.

Table 3 Integrated heat flux.

CH4: 2.2	52.1	[kW]
CH4: 2.6	51.2	[kW]
CH4: 3.0	50.8	[kW]
CH4: 3.4	55.5	[kW]
H2: 4.4	76.5	[kW]
H2: 5.2	73.6	[kW]
H2: 5.9	75.1	[kW]

3.3. Combustion Efficiency

The combustion efficiency in a liquid rocket engine is typically defined as

$$\eta_{c^*} = \frac{c^*_{exp}}{c^*_{id}}, \quad (1)$$

where c^*_{exp} is the actual value of the characteristic velocity determined from the experiment and c^*_{id} is the theoretical ideal characteristic velocity determined here using NASA's CEA code.

Two different efficiencies were determined from the experiment. The first one is the overall thrust chamber $\eta^{TC}_{c^*}$ efficiency and the other one the injector related energy release efficiency $\eta^{ER}_{c^*}$. Compared to the overall thrust chamber efficiency, in the determination of the ideal characteristic velocity for the energy release efficiency the enthalpy of the propellants entering the combustor has been corrected for the energy leaving the combustor through the wall, i.e. the integrated wall heat flux. The theoretically achievable characteristic velocity is therefore lower, due to the heat loss.

The combustion efficiencies calculated from the experimental data are shown in Fig. 7.

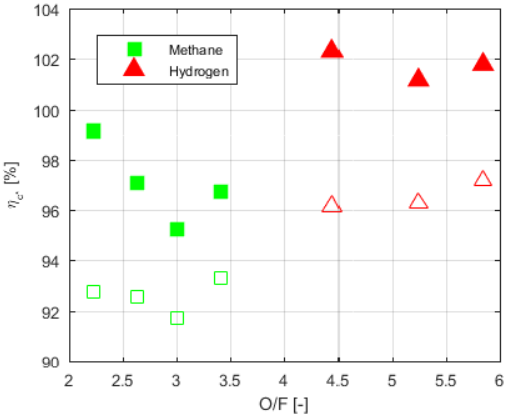

Fig. 7 Thrust chamber (non-filled markers) and energy release (filled markers) efficiency vs oxidizer to fuel ratio.

As can be seen the effect of the heat loss on the combustion efficiency, when taken into account, is quite substantial. For the hydrogen case the combustion efficiency is now over 100 percent, which theoretically is not possible. A probable reason for this behavior is the neglection of other effects that could potentially decrease the theoretically achievable characteristic velocity, such as chemical kinetic effects, two-dimensional flow features or boundary layer effects. Another possibility would be the deformation of the combustion chamber during the hot firing test and the in that case altered cross-sectional area of the throat. The investigation of the displayed behavior is still ongoing.

4. Numerical Results

As support for the interpretation of the experimental results two simulations, one for methane and one for hydrogen with a CFD model were performed. The results are presented here.

4.1. Model Setup

For the simulations the Reynolds-averaged Navier-Stokes (RANS) equations were solved on a computational grid of approximately 67000 cells. The domain contains the injector, chamber and nozzle and is seen as 2D axisymmetric. At the inlet the mass flow rates from the experiments are given together with the injection temperatures. The outlet is set to a supersonic pressure outlet. At the combustor wall the temperatures from the thermocouple readings are set directly. This is a slight underestimation of the actual temperatures, but the effect on the results from the simulation is assumed to be negligible.

Turbulence in both cases is modeled using a two-layer k-ε model. The wall is resolved to values of the dimensionless wall distance y+ of around one.

The combustion in case of methane is modeled using a laminar finite rate chemistry model, i.e. turbulence chemistry interaction (TCI) is neglected. As chemical kinetic scheme a 16 species 71 reactions mechanism[9] is used.

The combustion in case of hydrogen is modeled using an

equilibrium chemistry model based on the minimization of Gibbs enthalpy. TCI is modeled using an assumed beta PDF.

4.2. Results

The temperature field resulting from the simulations is shown in Fig. 8. The contour plots are in non-scale division.

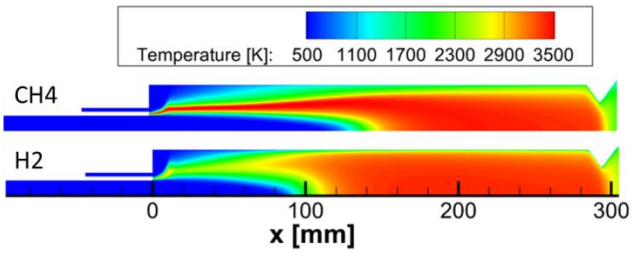

Fig. 8 Calculated temperature field.

Qualitatively distinct differences can be seen when comparing the methane and the hydrogen case. The cold zone originating from the oxygen inlet is shorter for the hydrogen case indicating a faster mixing and combustion. The hot zone for the methane case does not come as close to the wall as for hydrogen and seems to reach a more or less constant distance much later. The appearance of the temperature field is also clearly influenced by the combustion model used. In the methane case a very thin hot zone originates from the oxidizer post tip and broadens slowly until its crossing the chamber axis. For the hydrogen case the temperature of the hot zone originating from the post is lowered and 'smoothed' by the use of the PDF model for turbulence chemistry interaction.

These observations are also reflected in the calculated heat flux profiles shown in Fig. 9.

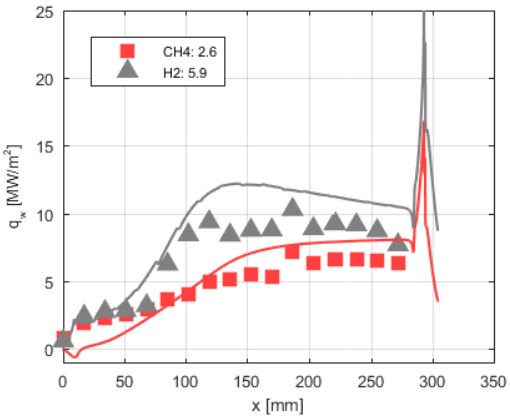

Fig. 9 Wall heat flux from CFD simulation vs experiment.

For the methane test case the heat flux is underestimated by the simulation up until about 100 mm into the combustor. Near the faceplate it is even negative due to cold methane from the injector being recirculated near the wall. The heat flux rises gradually as indicated by the temperature field until it reaches a plateau near the beginning of the nozzle. The plateau value from the simulation is higher than the experimentally determined value.

For the hydrogen test case the heat flux rise in the injector near region is predicted well by the simulation. The heat flux jump at 70 mm is also predicted by the simulation, even though slightly earlier. The heat flux after the jump is overestimated compared to the simulation and shows a decay in value due to the end of the combustion process.

The integrated heat fluxes are 57.7 kW and 95.0 kW for the methane and the hydrogen case respectively.

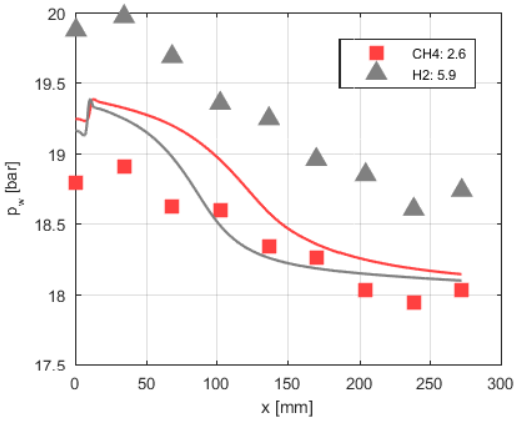

Fig. 10 Wall pressure from CFD simulation vs experiment.

The significant overestimation of the integrated heat flux in the hydrogen case leads to a, in comparison with the experiment, lowered pressure level, see Fig. 10. The wall pressure for the methane test case is predicted fairly well with a maximum deviation of less than 4 %.

Using the CFD results to calculate the combustion efficiencies in the same manner as described in section 3.3 the simulations can be thought of as "numerical experiments". The results are presented in Fig. 11.

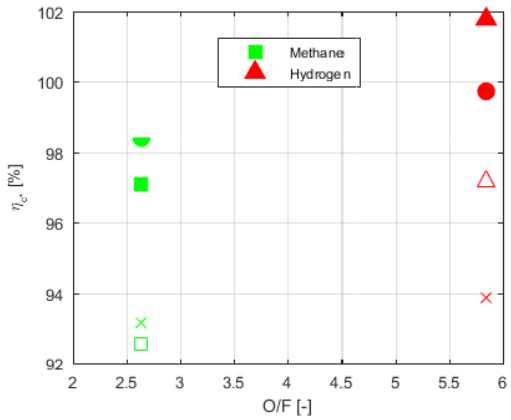

Fig. 11 Thrust chamber (non-filled square from experiments, cross from CFD) and energy release (filled square, circle from CFD) efficiency vs oxidizer to fuel ratio.

For the methane case both efficiencies are higher than the experimental ones indicating a better mixing in the simulation. The differences are lower than 2°% however. For the hydrogen case both efficiencies are lower than the experimental ones indicating a less effective mixing. It can also be seen that even

correcting for the over predicted integrated heat flux the nominal combustion pressure from the experiment cannot be recovered. Before the correction the difference is 3.3 %, after 2.1 %.

5. Conclusion

In the present work experimental results for a single element rocket combustor using a shear coaxial injector are presented. The combustor operates at 20 bar and uses gaseous oxygen as an oxidizer and gaseous methane or gaseous hydrogen as fuel. Seven different operating points are presented. Two of the load points are simulated using a RANS CFD model and the results are compared to the experiment.

In general the hydrogen tests result in a higher wall pressure level as well as a higher wall heat flux. Two combustion efficiencies were calculated for all load points, one overall efficiency and one corrected for the wall heat loss. In the hydrogen case the corrected efficiency exceeds 100°%. The reason for this is part of an ongoing investigation. Possibly this fact can be mitigated taken into account other effects when calculating the ideal characteristic velocity, e.g. chemical kinetic effects, two-dimensional flow features or boundary layer effects.

The simulations for the methane case show a fair agreement with the experimental data. Further model development is still ongoing. Especially a better agreement in the injector near region concerning the rise of the heat flux compared to the experiment is sought.

For the hydrogen test case the integrated heat flux is overestimated significantly which leads to a lower pressure level at the wall. However correcting for the heat flux still would not account for the whole pressure loss, as is suggested by an investigation of the predicted combustion efficiencies from the CFD analysis. The next step here is to simulate the hydrogen combustion using a chemical kinetic scheme instead of the equilibrium chemistry assumption.

Acknowledgments

Financial support has been provided by German Research Foundation (Deutsche Forschungs-gemeinschaft-DFG) in the framework of the Sonderforschungsbereich Transergio 40.

References

1) Burkhardt M., Sippel M., Herbertz A. and Klevanski. J.: A propellant tradeoff for reusable liquid booster stages, *Journal of Spacecraft and Rockets*, pp. 762-769, (2004).
2) Zurbach S., Thomas J., Vuillermoz P., Vingert L. and Habiballah M.: Recent advances on LOX/Methane combustion for liquid rocket engine injector, in AIAA 2002-4321, (2002).
3) Ueda S., Tomita T., Onodera T., Kano Y., Kubota I. and Munenaga T.: Hot-firing test of methane-fueled rocket engine under high altitude condition, in AIAA 2013-4056, (2013).
4) Schuff R., Maier M., Sindily O., Ulrich C. and Fugger S.: Integrated modeling and analisys for LOX/Methane expander cycle engine, in AIAA 2006-4534, (2006).
5) Schmidt G.: *Technik der Flüssigkeits-Raketenantriebe*, DaimlerChrysler Aerospace, (1999).
6) Celano M. P., Silvestri S., Pauw J., Perakis N., Schily F., Suslov D. and Haidn O.: Heat flux evaluation methods for a single element heat-sink chamber, *AIAA J.*, **10** (1972), pp. 1441-1447.
7) Johns Hopkins University: *JANNAF Rocket Engine Performance Test Data Acquisition and Interpretation Manual*, CPIA Publication, 245, (1975).
8) Gordon S., McBride B.: *Computer Program for Calculation of Complex Chemical Equilibrium Compositions and Applications*, Reference Publication NASA RP1311, (1994).
9) Sankaran R., Hawkes E.R., Chen J.H., Lu T.F., Law C.K.: Structure of a spatially developing turbulent lean methane–air Bunsen flame, *Proceedings of the Combustion Institute*, **31** (2007), pp. 1291–1298.